Experimental and numerical investigation of a taut-moored wave energy converter: a validation of simulated mooring line forces

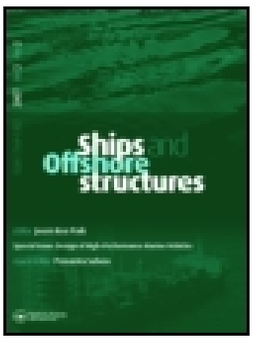

Taylor & Francis
Taylor & Francis Group

Ships and Offshore Structures

ISSN: 1744-5302 (Print) 1754-212X (Online) Journal homepage: https://www.tandfonline.com/loi/tsos20

Experimental and numerical investigation of a taut-moored wave energy converter: a validation of simulated mooring line forces

Shun-Han Yang, Jonas W. Ringsberg, Erland Johnson & Zhiqiang Hu

To cite this article: Shun-Han Yang, Jonas W. Ringsberg, Erland Johnson & Zhiqiang Hu (2020): Experimental and numerical investigation of a taut-moored wave energy converter: a validation of simulated mooring line forces, Ships and Offshore Structures, DOI: 10.1080/17445302.2020.1772667

To link to this article: https://doi.org/10.1080/17445302.2020.1772667

Published online: 31 May 2020.

SHIPS AND OFFSHORE STRUCTURES
https://doi.org/10.1080/17445302.2020.1772667

Taylor & Francis
Taylor & Francis Group

Experimental and numerical investigation of a taut-moored wave energy converter: a validation of simulated mooring line forces

Shun-Han Yang [a], Jonas W. Ringsberg [a], Erland Johnson [a,b] and Zhiqiang Hu [c]

[a]Department of Mechanics and Maritime Sciences, Chalmers University of Technology, Gothenburg, Sweden; [b]Department of Safety-Mechanics Research, RISE Research Institute of Sweden, Borås, Sweden; [c]School of Engineering, Newcastle University, Newcastle upon Tyne, United Kingdom

ABSTRACT

A reliable simulation model to calculate the motion and force responses of wave energy converters (WECs) is imperative to ensure the reliability and long-term performance of WEC systems; these aspects are fundamental to achieving full commercialisation of wave energy. A simulation model was developed and validated concerning the simulated WEC buoy motions in a previous study; this study validated the mooring force calculations for the same model. The example WEC system comprises a buoy, a power take-off (PTO) system, and a three-leg mooring system wherein each leg is divided into two taut segments joined by a submerged float. A 1:20 physical model was built and tested in the Deepwater Offshore Basin at Shanghai Jiao Tong University. Numerical models were developed to simulate the coupled hydrodynamic and structural responses of the WEC system, primarily using potential flow theory, the boundary element method, the finite element method, and the Morison equation. The simulated and measured axial force results at the top ends of the six mooring segments were compared; the results agreed best in the lower segments of each mooring leg and in the moorings on the downwind side because of the PTO system uncertainties and the uncalibrated damping in the numerical model. Nonetheless, the numerical model reasonably predicted the moorings' accumulated fatigue damage, demonstrating that the model can be reliably used for mooring structural analyses. The study also used the validated numerical model to simulate a full-scale WEC system installed in Runde, Norway. A comparison of the results from the full-scale measurements and simulations shows that the numerical simulation model exhibited a good predictive capability for the mooring forces of the full-scale WEC system.

ARTICLE HISTORY
Received 28 November 2019
Accepted 17 May 2020

KEYWORDS
Experiments; model validation; mooring forces; numerical simulation; taut mooring; wave energy converter

Nomenclature

H_s	Significant wave height [m]
H_w	Regular wave height [m]
N	Axial force in the mooring [N]
N^*	Dynamic axial force in the mooring. The value is shown with the initial static axial force (namely, the pretension force) subtracted. [N]
T_p	Peak wave period [s]
T_w	Regular wave period [s]
V_c	Current velocity [m/s]
γ	Non-dimensional peak enhancement factor of the JONSWAP spectrum [-]
η	Surface wave elevation [m]
θ_c	Direction of the current [degrees, °]
θ_w	Direction of the wave [degrees, °]

1. Introduction

The development of renewable wave energy technology relies heavily on numerical modelling and simulation because they provide flexibility to assess a large number of design choices for wave energy systems at a relatively low cost (Pecher and Kofoed 2017). Numerical simulation models for the simulation and assessment of hydrodynamic and structural responses for floating point-absorbing wave energy converters (WECs) were developed in Yang (2018); the objective of the model was to assess the power performance of WECs and the fatigue characteristics of mooring lines. The simulation model and numerical approach needed to be validated. Therefore, an experiment was designed and performed in an ocean basin laboratory at Shanghai Jiao Tong University in Shanghai (China) (SJTU 2019) with the objective of providing information to access the validity of the numerical analyses and the simulation models. Yang et al. (2018) presented the first part of the validation focusing on the simulated buoy motions—the responses for the evaluation of the power performance. From the maintenance and safety perspective, this second part of the validation study focuses on the calculated mooring forces—the essential information for predicting fatigue damage accumulation in moorings and their mechanical life. The contribution of the validation work is not limited to the scope of the current study; such a validated model can be used to provide confidence in the cost-efficient development of WEC systems, which is needed to reach large-scale commercialisation.

The experiment performed in this study aims to validate a previously developed numerical model presented in Yang et al. (2016). Guidelines for the experimental tests of WEC

CONTACT Shun-Han Yang Shunhan.Yang@chalmers.se Department of Mechanics and Maritime Sciences, Chalmers University of Technology, SE-412 96, Gothenburg, Sweden

systems have been considered by researchers such as Holmes (2009), ITTC (2014), Payne et al. (2009), and Pecher and Kofoed (2017). Although similarities can be found among these references, the ITTC guideline (2014) was followed because it provides clear guidance on the design, planning, and implementation of the numerical model validation experiment at both the system and component levels. A literature review presented in Yang et al. (2018) showed that numerous ocean basin tests have been conducted for various WEC systems and configurations. Advancing from the experimental tests reviewed in the cited reference, the experimental investigation in this study contributes to the research area of the two-segment taut mooring system (see an example illustration in Figure 1(a))—a mooring configuration that has been shown to have a high potential when used in WEC systems by virtue of its compliance in motion (Fitzgerald and Bergdahl 2007; Casaubieilh et al. 2014). In the present study, the two-segment mooring system was tested and validated in a complete WEC system where a power take-off (PTO) system is present, in contrast to existing studies where the mooring configuration has only been stand-alone tested (Bosma et al. 2015; Paredes et al. 2016).

Numerical models can be used to assist engineering developments with two different design philosophies. A numerical model can be carefully calibrated and fine-tuned to represent a system's responses under specific conditions and hence guarantee that the model exhibits the best predictive capability for the specific system. The other design philosophy is to develop a model that is generally applicable for similar systems. Under such circumstances, the numerical model is designed to provide a credible predictive capability without involving any calibration to a specific system. For the calculation of mooring forces, examples can be found for the former category, whereas few can be found for the latter. Xu et al. (2018) developed a model of a semi-submersible where the hydrodynamic drag and horizontal stiffness values of moorings were calibrated with laboratory measurements; the calibrated model predicted the damping effect of two mooring systems on the semi-submersible. Hall and Goupee (2015) developed numerical simulation models of a floating semi-submersible wind system to predict the hydrodynamic and structural responses. After a thorough model refinement, the lumped-mass mooring model predicted the extreme and fatigue damage-equivalent loads of the mooring with 90% accuracy. Harnois et al. (2015) presented a methodology to calibrate a numerical model of a WEC system based on a set of ocean basin experiments that further ensured a reliable prediction of the force responses of mooring lines for fatigue damage evaluations.

For the numerical models with the second philosophy, a generic model for the hydrodynamic and structural response analyses of moorings was developed in Azcona et al. (2017). In the cited reference, the model was developed only for the mooring component, which was excited by a prescribed motion at the mooring's top end. A model of the entire system including the moorings can be found in Antonutti et al. (2018) for wind energy applications. In their study, hydrodynamic coefficients were required as modelling inputs, which were all obtained by the designated physical measurements to minimise the model uncertainty. A robust dynamic simulation of catenary moorings is shown to be possible using their model provided that the inputs be organised consistently with the physics of offshore hydrodynamics.

However, there is a lack of validated numerical models for complete WEC systems in the literature. In addition, the goal of the developed model in Yang (2018) was to be generally applicable for various WEC systems in the early design phase; the detailed model measurements presented in Antonutti et al. (2018) were thus deemed unpragmatic and should not be included as part of the validation process. The observed lack of validated models with similar evaluation purposes motivates the need of the present study. This validation work was performed with regard to the calculated axial forces in the moorings, whereas the assessment criterion was set to achieve the predictive capability of the accumulated fatigue damage within a factor of ten. The criterion was determined by considering the associated uncertainty level of fatigue for the floating offshore structures (DNV 1992; Aker Offshore Partner 1999). The novelty of the presented work is that the entire WEC system was numerically modelled with inputs from only the physically designed parameters and numerical coefficients estimated exclusively from existing public literature and that no calibration of the simulation model was performed.

The primary objective of the current study was to validate the simulation procedure and numerical model with regard to the force response analysis against the results of ocean basin laboratory tests, as presented in Sections 2 and 3. In this validation work, the comparison of the validation result was performed exclusively on the experimental model scale, i.e. there was no transformation of the values to full-scale values in the comparison between the simulation and experimental results. After validation, the numerical simulation model was adapted to be similar to a full-scale WEC installation to demonstrate the model's prediction capability against the full-scale measurements; this process is presented in Section 4 and serves as the second objective of the study. Finally, Section 5 presents the observations and conclusions from the current investigation.

A prototype device, WaveEL, which was designed by the Swedish company Waves4Power (Waves4Power 2019), was chosen as the reference concept for the entire validation study and was installed in full scale in Runde (Norway) in early 2016. Figure 1(a) illustrates a schematic view of the WaveEL system, and a photograph of the installation site is presented in Figure 1(b). The system consists of a floating point-absorbing WEC that extracts energy from waves, primarily from heave motions. The WEC is moored by a three-leg mooring system where each leg is divided into two taut segments joined by one float, wherein the float is designed to be submerged at all times. The power generated by the WEC is transmitted to a power-gathering hub through a power cable. The cable is submerged and designed to operate in a free-hanging state between the WEC and hub. The hub has a single-leg taut mooring system that is designed to keep the hub in a stationary position.

2. Experimental setup for the ocean basin tests

The ocean basin experiment was designed to be as similar as possible to the full-scale installation (see Figure 1); the experiment was conducted in the Deepwater Offshore

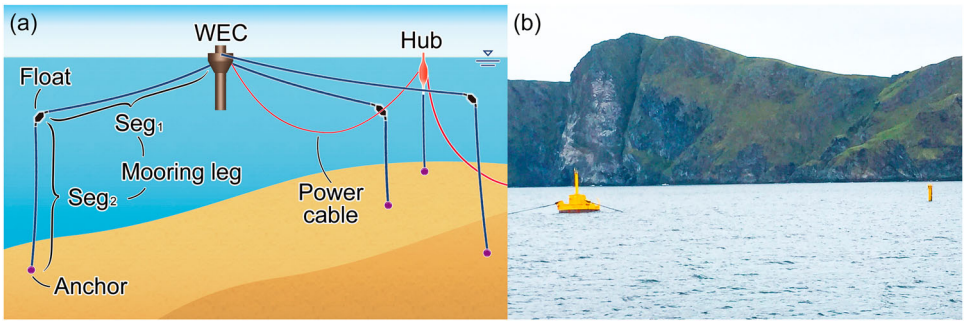

Figure 1. (a) Schematic layout of the WaveEL system and (b) photograph of the full-scale installation in Runde, Norway.

Basin at Shanghai Jiao Tong University. As addressed in ITTC (2014), the responses and performances of WECs are normally scaled using Froude similitude, but exceptions occur for parameters such as the power output, viscous damping, and mechanical friction; large-scale test models are recommended to minimise the scaling effect. To that end, a 1:20 scale model following Froude's law was chosen for experiments with sea states corresponding to operational conditions. Considering the configuration of the reference system and the sea state conditions to be tested, the ratio of 1:20 was the largest possible scale for the ocean basin. Yang et al. (2018) present a complete description of the ocean basin experiments, whereas information that is relevant for this paper is presented in Sections 2.1 and 2.2 with corresponding numerical values tabulated in Tables A1–A3. The numerical model and simulation of the experiments are presented in Section 2.3.

2.1. Design of the experimental WEC system

Figure 2 illustrates the experimental WEC system, which consists of a WEC buoy, a PTO system, and a three-leg mooring system. The power cable shown in Figure 1 was excluded to maintain an acceptable level of complexity in the experimental system. The WEC buoy was a closed buoy. The mass, centre of gravity (CoG), and inertial properties of the reference system were used as the target values for the experimental model. The entire experimental PTO system consists of a heave plate, a connection bar, and a helical spring. The heave plate acts as a damper in the WEC system, and its target damping effect at the full scale was chosen in a way that yields the optimal PTO of the WEC when the damper is at the resonance in the heave motion degree of freedom (DoF). The usage of the connection bar ensured the movement of the heave plate followed the buoy's motion, and the spring enabled force measurements for the heave plate.

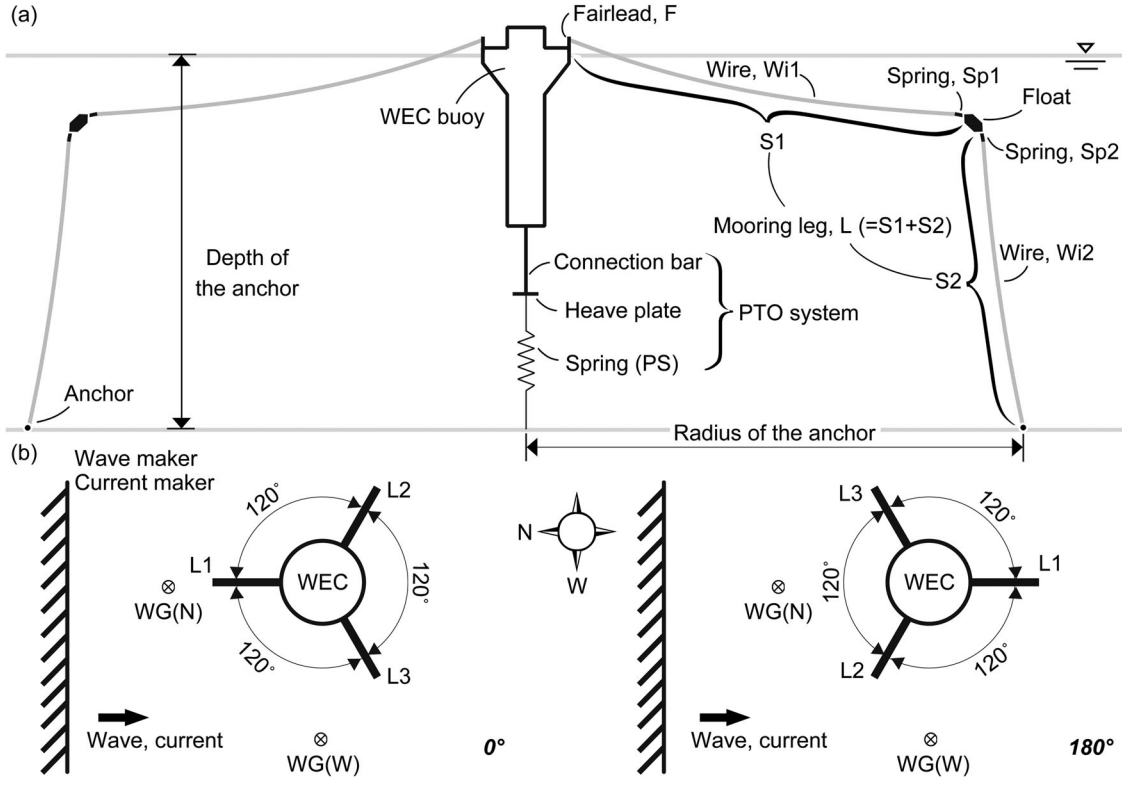

Figure 2. Illustration of the configuration of the WEC system for the ocean basin experiment (not to scale): (a) profile view and (b) top view for the loads coming from the directions of 0° (left) and 180° (right). The wave gauge is referred to as WG in the figure (figure reproduced from Yang et al. (2018)).

Each mooring segment in the full-scale prototype was represented by a combination of one wire and one helical spring. Four properties of the mooring were modelled in the experimental system: axial stiffness, length, pretension force, and submerged weight. For these four properties, the combined effect of every set of one wire and one spring at full scale were designed to be equivalent to the respective properties of the corresponding segment in the reference system with only one exception. During the installation, the exact final installed length of wires at the three upper segments (Wi1) was adjusted to achieve the target pretension force at the full scale.

Multiple sensors were installed to monitor and measure the dynamic responses of the experimental system; see an overview of the instrumentation in Figure 3. The force measurements at the upper ends of all six segments in the mooring system (Figure 3(d) and 3(e)) and the top end of the PTO's spring (Figure 3(b), hereafter referred to as PS) were used in the experiment, from which the dynamic force responses of the moorings are to be validated. All forces were measured by KYOWA LUX-B-100N-ID force transducers at a sampling frequency of 25 Hz; the measurement accuracy of the transducers is one millinewton (KYOWA 2019).

2.2. Environmental condition – test programme

Table 1 presents all the loading conditions investigated in the current study, which correspond to the operational conditions of the reference system. Both regular and irregular wave cases were included in the test programme. For the regular wave cases, T_w values were chosen to be identical to (Re3-Re5), near (Re2 and Re6), and far from (Re1 and Re7) the resonant period of the unmoored WEC buoy. Then, the H_w values were determined such that they cover the range between linear (Re1-Re3 and Re6-Re7), nonlinear (Re5), and intermediate (i.e. between linear and nonlinear) (Re4) waves. The distinction of waves was evaluated by the ratio of the wave height and wave length following the definition of Chakrabarti (1987). For the irregular wave cases, the OP1-related case was defined as the optimum operation condition for the installed WEC system because this case approximates the WEC resonance period and because the probability of occurrence for this case is high at the installation site in Runde. In contrast to OP1, case OP2 was chosen to be off the resonance of the unmoored WEC buoy. Note that case OP1 was also tested in greater detail to investigate the effects of the loading direction ($OP1_d$), the wave-current combined loads ($OP1_c$), and the PTO system ($OP1_n$). All the regular wave cases were tested for 10 min at full scale, the case Curr was tested for 45 min, and the irregular wave cases were simulated for 1.5 h at full scale.

2.3. Numerical model and simulated experiments

The purpose of numerical models is to predict the hydrodynamic and structural responses of WEC systems. From the motions, hydrodynamics, and structural response of a simulated WEC system or an array of WECs, the numerical models enable a systems evaluation of the WEC system in which the fatigue performance of moorings and cables is predicted, the power performance is estimated, and the cost of energy is calculated. A literature survey was conducted by Yang (2018) to compare the advantages and disadvantages of different model and analysis approaches, particularly with regard to the fatigue damage assessment of mooring lines used for wave energy applications. It was concluded that the numerical implementation used by the DNV GL SESAM package (DNV GL 2019) facilitates the modelling and assessment of the WEC, the mooring lines, and the power cable (all exposed to a variety of environmental conditions) in a manner suitable for the defined research scope. The modules and solvers in the SESAM package have also been extensively verified and validated by numerous researchers; see, e.g. Ormberg et al. (1999) and Stansberg et al. (2000a, 2000b). The DNV GL SESAM package was adopted to create the model and to perform the numerical analyses.

Figure 4 illustrates the numerical model of the WEC system. The model is composed of six sub-level models, which are used together to simulate the system's hydrodynamic and structural responses. An overview of the six sub-models is presented in Table 2, and the entire analysis workflow is illustrated in Figure 5. As shown in Yang et al. (2016), the coupled analysis approach, which solves both the WEC and the moorings simultaneously using nonlinear time-domain analysis, yields more accurate results than the de-coupled approach for the motion response of the WEC and structural responses of the moorings and was therefore used in this study. The coupled analysis approach performs nonlinear analysis comprising four major sources of nonlinearity, including the geometric stiffness of the mooring system, displacement dependencies of the moorings regarding the inertia and damping forces, coupling between the external load vector and the structural displacement and velocity, and nonlinear time-domain analysis. The application of the SESAM package and the comparison of different approaches for simulating WEC systems were extensively investigated in Yang (2018) and Yang et al. (2016), in which detailed descriptions of the theoretical background, modelling details, and numerical parameter setup can also be found.

Prior to the current validation exercise, the uncertainty of the numerical model related to the setting of numerical parameters (e.g. element discretisation, time step size) was verified through a convergence sensitivity study. Note that the numerical model used in this investigation is identical to the one used in the first part of the validation study (presented in Yang et al. (2018)) with only one exception, the length definition of Wi1. In the previous validation work, the numerical model for the moorings was defined according to the designed target length, and the pretension force was dependent on the length. However, it was later clarified that the pretension force at the top end of S1 takes precedence over the final installed length of Wi1 during the installation. To ensure the same modelling principles between the simulations and experiments, the numerical model was updated in this study so that the simulated pretension force was identical to the target pretension used during the experiments (viz., the length of Wi1 becomes a dependent variable). Further investigation has shown that all the conclusions made in Yang et al. (2018) remained true, and relevant discussion will be presented in Section 3.

3. Validation results for the ocean basin test

This section presents a selection of results from the validation study that are representative of all studied cases, starting with

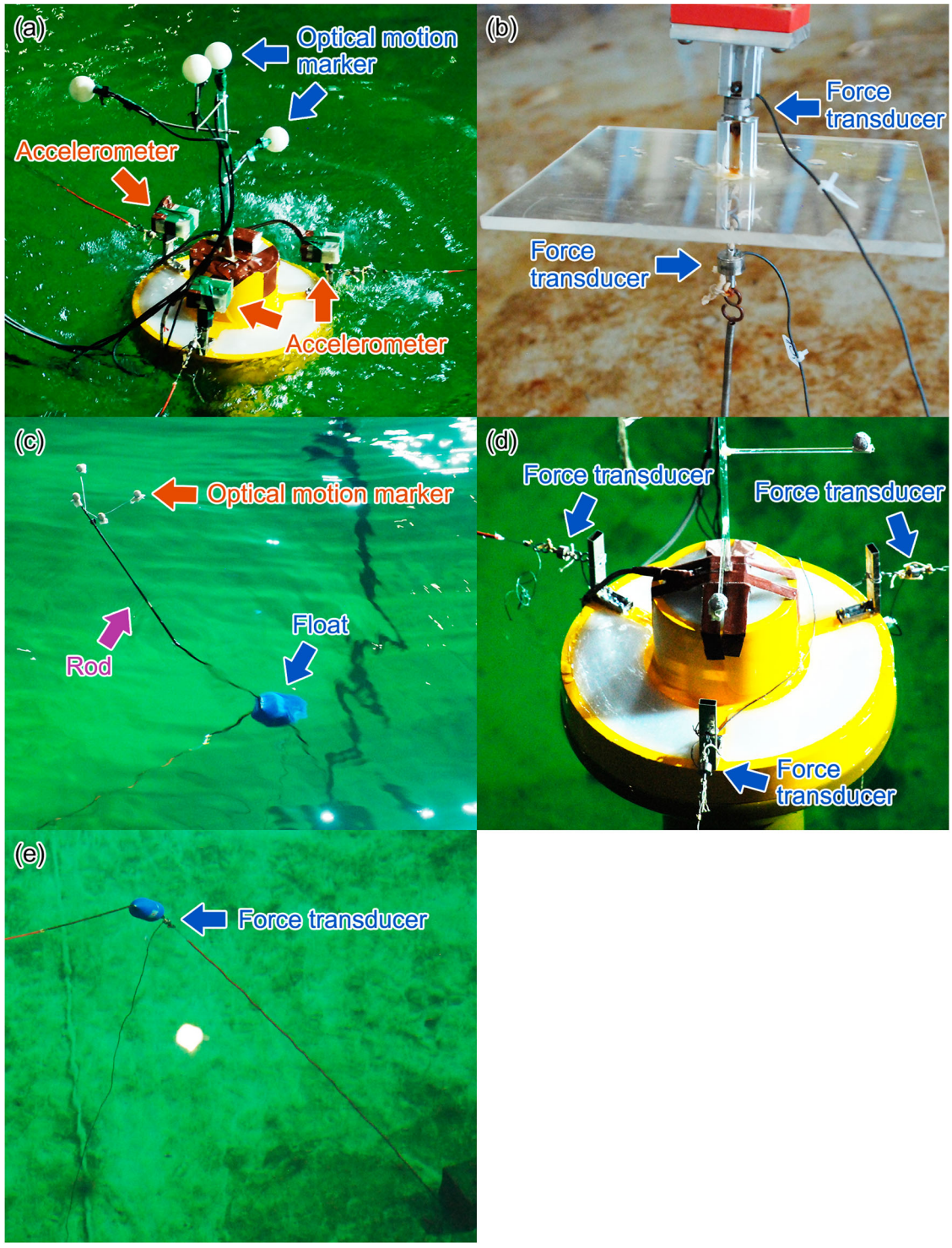

Figure 3. Instrument installation in the WEC system: (a) optical motion markers at the upper deck of the WEC buoy and accelerometers at the fairlead of the three moorings; (b) force transducers on the upper and lower sides of the heave plate used in the PTO system; (c) optical motional markers on the upper end of the rod, which attaches to the float; (d) force transducers at the fairlead of each mooring leg; and (e) force transducer on the upper end of the lower mooring segment (figure reproduced from Yang et al. (2018)).

the results for the static characteristics of the mooring system (Section 3.1) followed by the dynamic results from regular (Section 3.2) and irregular wave (Section 3.3) cases. As discussed in Yang (2018), because the stress level of the target mooring is considerably lower than its design yield stress, a stress-based approach can be adopted in the fatigue analysis, and only the force range of each force cycle (and consequentially, each stress cycle) identified from the mooring's time-domain response will have an influence on the fatigue calculation, along with the mooring's own fatigue material properties. After validating the axial force calculation, the model can be reliably used for fatigue damage prediction. The results presented in Sections 3.2 and 3.3 (the dynamic results) will only focus on the comparison of the force range of the identified force cycles. In this study, the

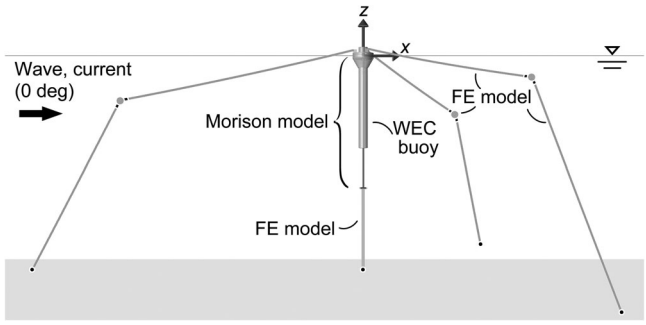

Figure 4. Initial configuration of the numerical model.

rainflow counting (RFC) method is employed to extract the force cycles from the force history and the corresponding force ranges for the fatigue analysis (Rychlik 1987; Dowling 2013); a detailed procedure of the stress and fatigue analysis for moorings is presented in Yang et al. (2016).

3.1. Pretension and static offset of the mooring system

Table 3 shows all the force measurements and corresponding simulated values under still water conditions. This information reveals the potential discrepancy with regard to the static restoring force of the mooring system between the experiments and numerical simulations. Different experimental results for the same components between cases are due to re-installation of the system in the ocean basin. The simulated results agree well with the measurements, and the minor discrepancies were attributed to two factors: mooring length uncertainty and PS configurations.

Both the numerical model and experiment were defined to achieve the target pretension force (see Section 2.3 and Table A2). Given a symmetrical system, identical lengths of Wi1 among the three mooring legs are expected in the numerical model. The lengths of Wi1 for the three mooring legs were adjusted one after the other in the experiment. Table 3 shows different pretension forces between the segments; hence, different installed lengths among segments were expected. A similar issue was also observed in other experimental studies, which motivated the calibration of the mooring length in the numerical model (see the example in Hall and Goupee (2015)). In this study, however, calibration was not allowed as the prerequisite of the investigation (see Section 1); hence, this intrinsic difference between the simulation and experiment will be maintained throughout the entire validation work.

Table 1. Summary of the tested wave and current scenarios in full scale (FS) and model scale (MS) values.

		T_w or T_p		H_w or H_s		V_c		θ_w and θ_c**
Case name	Regular or irregular waves*	FS [s]	MS [s]	FS [m]	MS [m]	FS [m/s]	MS [m]	FS and MS [°]
Re1	Regular	3.185	0.712	0.238	0.012	–	–	0
Re2	Regular	5.370	1.201	0.675	0.034	–	–	0
Re3	Regular	6.370	1.424	0.950	0.048	–	–	0
Re4	Regular	6.370	1.424	1.900	0.095	–	–	0
Re5	Regular	6.370	1.424	3.801	0.190	–	–	0
Re6	Regular	7.370	1.648	1.272	0.064	–	–	0
Re7	Regular	12.740	2.849	3.679	0.184	–	–	0
OP1	Irregular	6.500	1.453	2.500	0.125	–	–	0
$OP1_d$	Irregular	6.500	1.453	2.500	0.125	–	–	180
$OP1_c$	Irregular	6.500	1.453	2.500	0.125	0.514	0.115	0
$OP1_n$***	Irregular	6.500	1.453	2.500	0.125	–	–	0
OP2	Irregular	9.600	2.147	4.500	0.225	–	–	0
Curr	–	–	–	–	–	0.514	0.115	0

* A regular wave is defined by T_w and H_w, while an irregular wave is defined by T_p and H_s. All irregular waves follow the JONSWAP spectrum, wherein γ is set to 2.4.
** The definition of the loading direction in relation to the orientation of the WEC system is shown in Figure 2.
*** The test condition of $OP1_n$ is the same as that for OP1 except that the PTO system is removed in $OP1_n$.

Table 2. Overview of the six sub-level models used for the numerical analysis.

Sub-model	Information of the WEC system to be extracted from the simulation	Applied theory	Steps to be used in the workflow (cf., Figure 5)
Environmental load model	External environmental loads acting on the WEC system	Airy wave theory; unidirectional current (time- and depth-invariant)	All steps
Panel model of the WEC	Hydrostatic data and inertia properties of the WEC buoy; global responses of the WEC buoy in frequency domain, including the hydrodynamic added mass and damping, first-order wave exciting forces and moments, and second-order drift forces and moments	Boundary element method; first- and second-order three-dimensional potential theory	Step 1
Point model of the WEC	First- and second-order motion and force response of the WEC buoy in the time domain	Rigid body motion; retardation function; Newmark β time stepping scheme	Steps 2 and 3
Morison model of the PTO system	Drag damping effect of the PTO system	Morison equation; two-node beam element model	All steps
Morison model of the WEC	Drag damping effect of the WEC buoy	Morison equation; two-node beam element model	All steps
Finite element model of the moorings	Time-domain motion and force response of the mooring systems	Morison equation for hydrodynamic loads; continuum mechanics theory for structural response; two-node beam element model based on small strain theory; Newmark β time stepping scheme	Steps 2 and 3

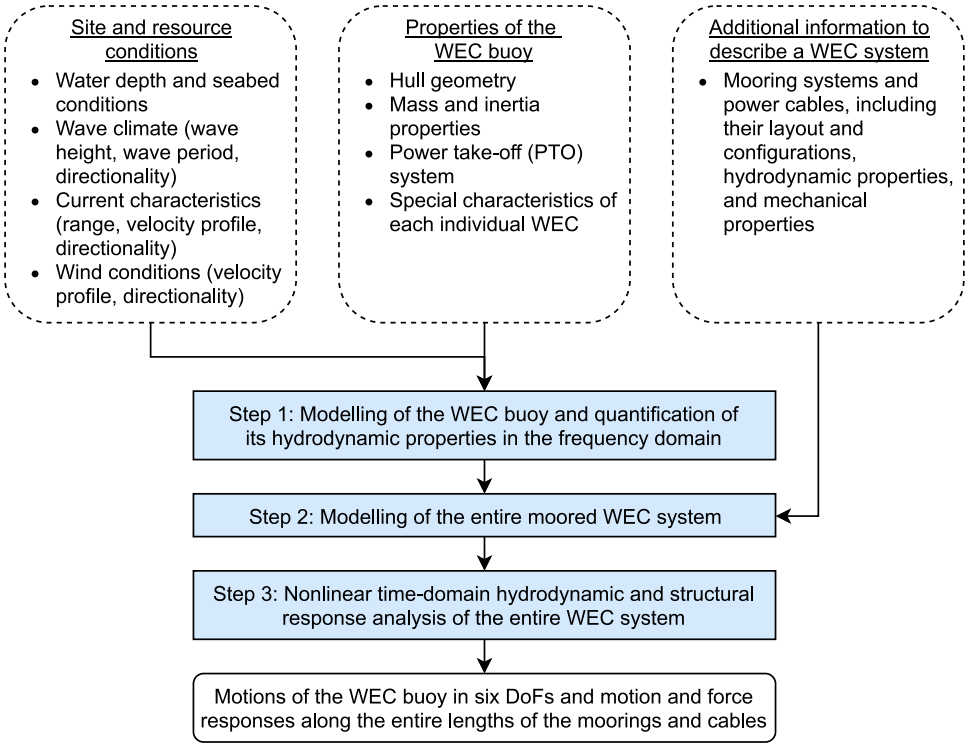

Figure 5. Analysis workflow for simulating the hydrodynamic and structural response of WEC systems.

Table 3. Force measurement (the first value is from the experiment, and the second value is the ratio between the values of the simulation and experiment) at the top ends of all components under still water conditions. The simulation results for segments S1 and S2 are 2.683 and 7.367 N, respectively, and are identical among the three mooring legs in all cases; similarly, the calculated value for PS is 3.478 N.

Case	L1S1	L2S1	L3S1	L1S2	L2S2	L3S2	PS
Re1 – Re7, OP1	2.565/1.05	2.657/1.01	2.673/1.00	7.166/1.03	7.105/1.04	7.037/1.05	3.242/1.07
$OP1_d$	2.662/1.01	2.617/1.03	2.714/0.99	7.173/1.03	7.091/1.04	7.180/1.03	3.302/1.05
$OP1_n$	2.638/1.02	2.707/0.99	2.730/0.98	7.149/1.03	7.131/1.03	7.300/1.01	–
$OP1_c$, OP2, Curr	2.812/0.95	2.543/1.06	2.824/0.95	7.135/1.03	7.071/1.04	7.154/1.03	3.285/1.06

Nevertheless, the agreement was determined to be good for the pretensions of all the mooring segments since the difference between the measured and simulated results was always less than 5%.

In contrast, the agreement was less satisfactory regarding the PS, where the PS pretension predicted by the numerical simulation was an average of 7% greater than the experimental values; this overprediction is attributed to uncertainty in the PS installation configuration, which is regarded as a second source of uncertainty. The properties of the installed PS were measured for only the spring constant and unloaded length, whereas the geometrical dimensions and mass density were also needed to fully define the PS in the numerical model. Hence, estimations of the PS's properties were made using the spring calculator developed by Acxess Spring (Acxess Spring 2019). The other challenge presented by the PS is the use of two springs connected in series rather than a single spring to represent the PS because a proper single spring for the target length and axial stiffness was not available. Due to the unbalanced force between the three moorings, it is difficult to ensure that the two springs remained in a straight line. In the numerical simulation, however, the PS deformation will always be vertically straight-up under the still water condition because of the symmetry. Nevertheless, the overall results observed under static conditions were deemed reasonable.

The horizontal offset of the mooring system under statically applied force is shown in Figure 6, from which the restoring capacity of the mooring system can be compared between the experiment and simulation model. Note that the simulation results presented in Figure 6 are different from those presented in Yang et al. (2018); this difference was due to the update of the numerical model described in Section 2.3. Excellent agreement between the simulation and experiment was found for the offset of the mooring for the sway direction. Good agreements were also found for the surge direction in the low-load region but not the high-load region (i.e. forces above 5 N), where the simulated mooring offset in the latter is higher by up to 40%. The difference was attributed to the complexity in the installed mooring system in conjunction with the necessary abstraction in the numerical model, as shown in Yang et al. (2018). Overall, the updated model shows an improvement in the prediction of the horizontal offset of the mooring system. Further investigations showed that the simulated WEC motion was insensitive to the model change, and hence, all the conclusions made in Yang et al. (2018) are still valid. Because the updated model better represents the scenario of the experiment, this model was used henceforth.

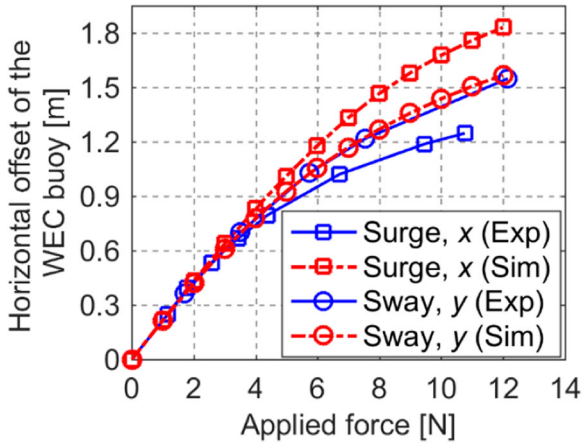

Figure 6. Static offset of the mooring system in the horizontal plane (surge and sway direction).

3.2. Regular wave cases

Figure 7 presents the time-domain results of the force responses of the mooring system (Figure 7(a)-(f)) and PS (Figure 7(g)) for case Re1. The displayed values, denoted as N^*, are shown with the pretension force (namely, the initial static forces shown in Table 3) subtracted. Because all the force sensors were zeroed before the start of the dynamic measurements, the presented experimental results are the direct readings from the sensors. The corresponding surface wave elevation for the same time duration is plotted in Figure 7(h). Note, however, that the experimental results were extracted from the measurements at the wave gauge WG(N) (see Figure 2), and the simulated results were extracted at the geometrical centre of the waterplane of the buoy under still water conditions.

The overall agreements between the calculated and measured mooring forces were satisfactory, but the level of prediction accuracy differed among the mooring segments. Because the numerical simulation underestimated the load in the PS, the force amplitude in L1 was overestimated. The correlation was tied to the fact that both L1 and PS were located on the windward side of the system. The ratios between the simulated and measured force ranges were found to be 1.15 for L1S1 and 1.41 for L1S2. In contrast, the simulated axial forces agree very well with the measurements for L2 and L3. Comparing the force responses between L2 and L3 from the simulations and experiments, symmetrical responses were observed between L2 and L3 from the numerical simulation but not from the experiment; the cause of the asymmetry was attributed to the installation of a motion tracker at the joint between Sp1 and the float in L2, as shown in Figure 3(c). A sensitivity study presented in Yang et al. (2018) showed that the buoy motion was insensitive to the motion tracker; however, further investigation revealed the impact of the tracker on the motion and force responses of L2. One example result is shown in Figure 8, where the force responses of L2S2 and L3S2 under case Re7 are compared considering the influence of the motion tracker. As shown in Figure 8(b), when the motion tracker was installed, the mean value of the force response in L2S2 was smaller by 0.1 N, the force range was reduced by 5%, and the structure exhibited more high-frequency fluctuations at both the crest and trough of each force cycle at the wave frequency. Focusing on the comparison for L3, the relative differences between the simulation and measurement were less than 5% for both segments. Finally, the simulated phase differences between the mooring segments are in accordance with the measurement results, implying a good prediction from the numerical simulation of the system's inertia and restoring forces.

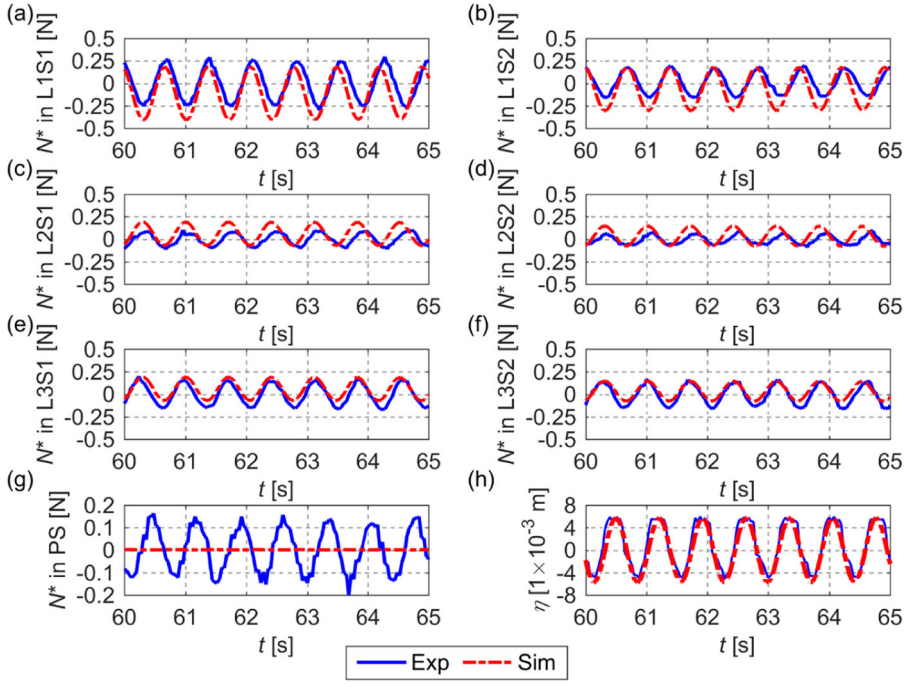

Figure 7. Time histories of the dynamic responses N^* under case Re1: (a – f) top ends of the six mooring segments, (g) top end of the PS, and (h) surface elevation of the wave.

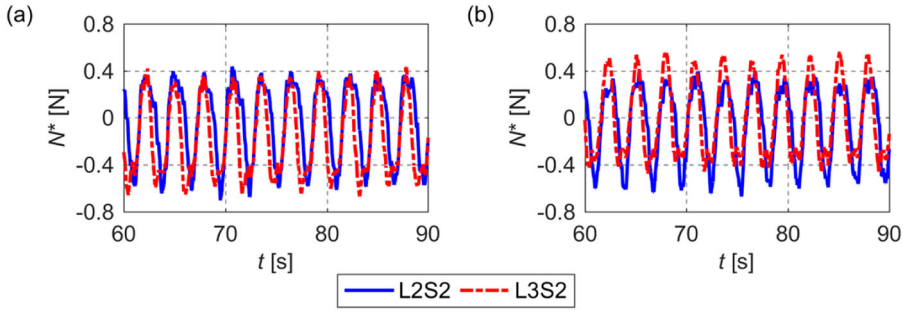

Figure 8. Time histories of the dynamic responses N^* of L2S2 and L3S2 under case Re7 (a) without and (b) with the installation of the motion tracker.

For a harsher wave load condition, the results for case Re7 are presented in Figure 9. In this case, however, a clear phase difference was observed between the simulated and measurement force responses; this difference was attributed to the fact that PS was not always in tension (see Figure 9(g)). In fact, frequent compressions of the PS were found in all the tested cases except case Re1—a situation not anticipated prior to the experiments. The moorings in the numerical model were constrained to exhibit stiffness in the axial direction only, which was found to be the best representative case for moorings in most offshore structures, including WECs (DNV GL 2015; Hall et al. 2014). Under this modelling condition, however, if compression of the mooring occurred, the basic analysis criteria of DNV GL software were violated, and the numerical simulation ceased (SINTEF Ocean 2018). The usability of the experimental data for validation purposes is then largely compromised because the experiment was not suitable for the simulation method. Simulation of a slender structure (such as the moorings in this study) at low tension is in itself a research subject. The tension element method, for instance, is one of the numerical methods developed to simulate slender structures with low pre-stressing or high flexibility (Paschen et al. 2004; Martin et al. 2018). Other simulation approaches have also been proposed by, e.g. Buckham and Nahon (2001) and Burgess (1992). A possible research extension is to explore the use of these aforementioned numerical methods to increase the usability of the experimental results. In this study, however, the focus is on validating the previously developed numerical methods and models (see Section 2.3); no other numerical method is thus adopted.

The force measurements of the PS, together with the measurement at the top side of the heave plate (c.f. Figure 3 (b)), provide information about the forces in the PTO system. This information can normally be used to study the WEC performance in detailed time-domain analysis. In the current study, however, there were uncertainties related to the PS regarding its mechanical properties; see Section 3.1 for a discussion. Because of these uncertainties, it was known at the outset of the study that the dynamic response results of the PS could not be included in the validation. Nevertheless, because the

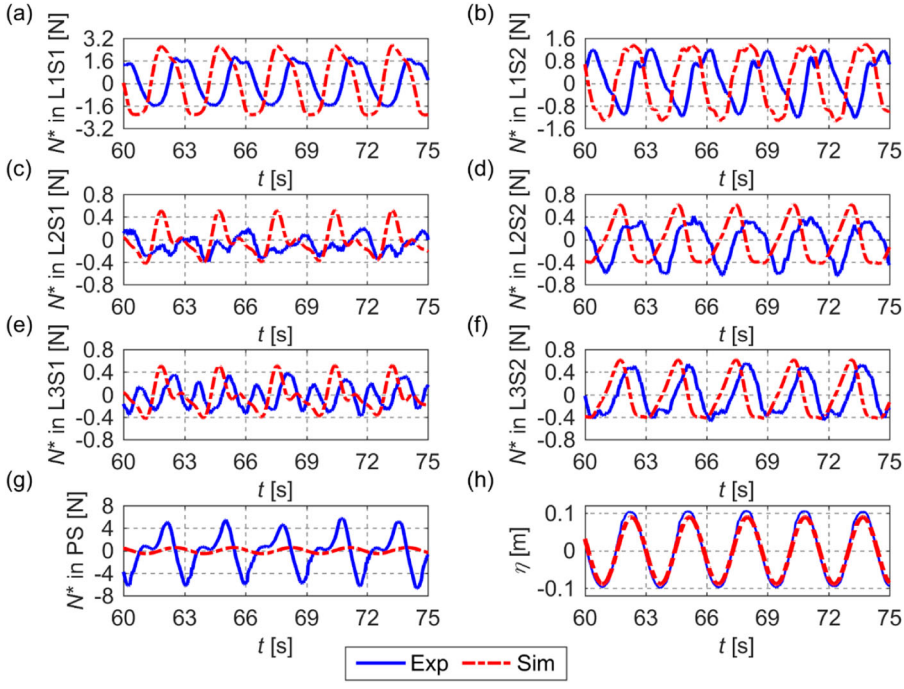

Figure 9. Time histories of the dynamic responses N^* under case Re7: (a – f) top ends of six mooring segments, (g) top end of the PS, and (h) surface elevation of the wave.

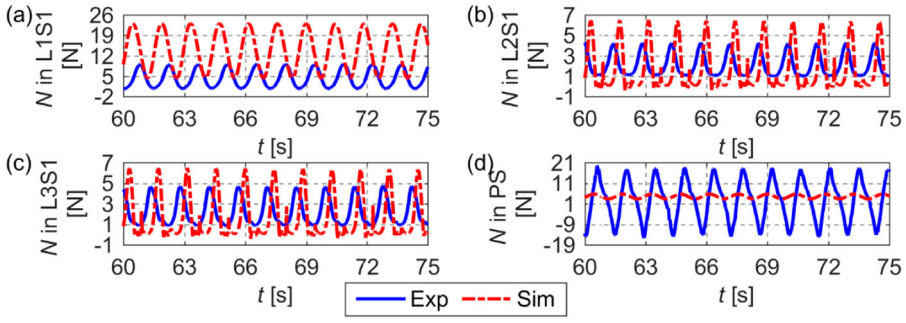

Figure 10. Time histories of the dynamic responses *N* under case Re5: (a – c) the top ends of three mooring upper segments S1 and (d) the top end of the PS.

current model was designed for a simplified power performance prediction that requires only the validated buoy motions and the predefined damping coefficient of the PTO system for the calculation, the numerical model was deemed acceptable for its original goal of the power estimation.

The uncertainty of the PS will have an even larger impact under harsher loading conditions when the external wave load is substantially larger than the initial pretension force in the moorings and PS. An illustrative example is presented in Figure 10 from case Re5, which is the most severe loading condition tested in this experiment. Note that the results presented in Figure 10 are the absolute values of the axial force, *N*, in each respective component (namely, the pretension force was not subtracted) to better compare the real magnitudes of the forces between the components.

The results for case Re7 (Figure 9) demonstrated that the numerical simulation is able to capture not only the primary force cycles but also the detailed response characteristics. Taking examples from L1, despite its inherent challenge for an accurate prediction (see discussions regarding Figure 9), small details in each force cycle are well predicted by the numerical simulation. Thus, one can observe superimposed high-frequency fluctuations at the crest of each force cycle at the wave frequency. In addition, the responses showed hysteresis at the trough of each main cycle for L1S1 but not for L1S2. Such information is important for the prediction of force cycles that lead to a reliable estimation of the accumulated fatigue damage.

The predicted axial force from the numerical simulation is generally larger than those from the experiments, and the difference increases as the wave condition becomes closer to the system's resonance. This phenomenon is attributed to buoy motion. Figure 11 shows the response amplitude of the buoy motion as ratios between the simulation and experiment, where the corresponding absolute values can be found in Yang et al. (2018). Comparing Figure 11 with the other results in Figures 7–10, correlations for the predictive capability of the numerical model were evident between the simulated buoy motion and force responses. The reason for the discrepancy between the simulated buoy motion and the experiment was discussed in Yang et al. (2018), wherein two causes were identified. First, the WEC damping was considered numerically as radiation damping and linearised drag damping, which cannot sufficiently account for the frequency dependency of the viscous damping. A demonstrative example was presented in Yang et al. (2018), which showed a good resemblance of the simulated motion after the model calibration. Second, nonlinear responses of the WEC system were observed from the experiment due to the presence of overtopping and vortex-induced motion—both of which cannot be simulated by the linear solvers used in the SESAM software.

As the last point of observation for all the regular wave cases, good agreements were always found between the simulation and experiments for all the lower segments Sp2; the average ratio between the simulated and experimental axial forces was 1.2. The design principle for the tested mooring system was to enable large WEC motions through the nearly horizontal and compliant mooring attachment at the upper segments while simultaneously minimising the excursion of the mooring in the lower segment. Hence, irrespective of the uncertainties in the PS and buoy motions, the force responses in the lower segments are mainly governed by their own initial configurations and the external environmental loads. The good agreement between the simulations and experiments demonstrates that the numerical model is able to correctly predict the force response of the moorings under a well-controlled loading environment together with a good understanding of the moorings' configurations and mechanical properties.

3.3. Irregular wave cases

Among all the tested loading conditions, $OP1_n$ is the case without the PTO system and therefore can be used to verify the factors underlying the uncertainty in the PS discussed in Sections 3.1 and 3.2. Figure 12 presents a histogram of the force cycles identified for $OP1_n$ and OP1. The results from segments L1S1 and L3S2 were plotted since they are considered to be most prone and least prone to the influence from the PTO system, respectively. As expected, agreeable results between the

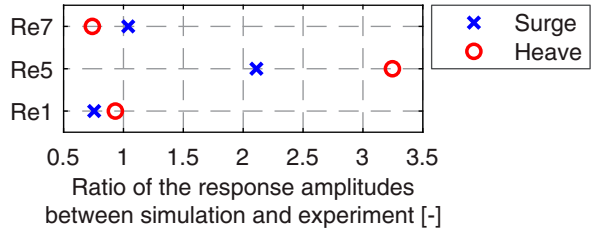

Figure 11. Comparison of the response amplitude of the buoy motion in the simulation to that in the experiment; the absolute values of the data can be found in Yang et al. (2018).

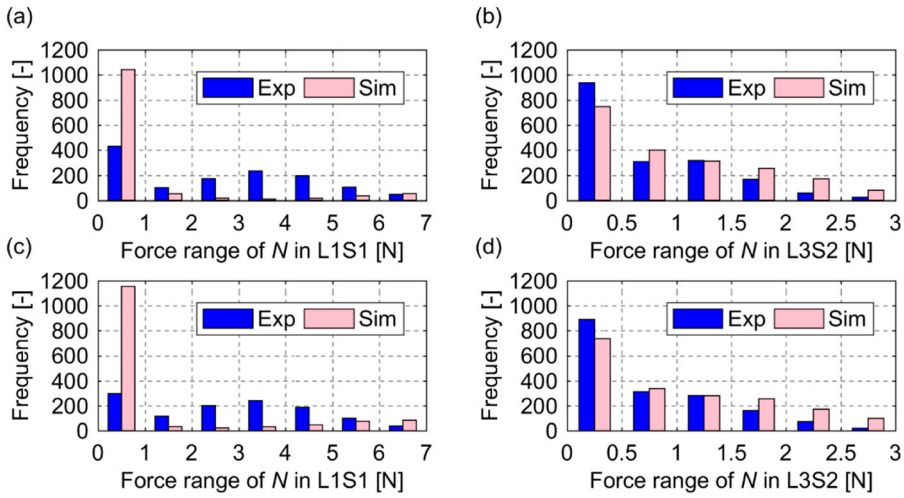

Figure 12. Force range histograms of the mooring segments: (a) L1S1 and (b) L3S2 under $OP1_n$ and (c) L1S1 and (d) L3S2 under OP1. The horizontal axis shows the force range of each force cycle identified in the time history of the mooring responses, and the vertical axis shows the frequency of occurrence during the entire test duration.

Table 4. Estimated fatigue damage for the six mooring segments in cases OP1, $OP1_n$, and OP2. The fatigue material properties m and a in the S-N curve are set to 3 and $10^{12.163}$, respectively (DNV GL 2015).

Case		L1S1	L2S1	L3S1	L1S2	L2S2	L3S2
$OP1_n$	Exp	4.1×10^{-10}	1.8×10^{-10}	1.8×10^{-10}	3.3×10^{-10}	1.3×10^{-10}	1.5×10^{-10}
	Sim	9.1×10^{-10}	3.7×10^{-10}	3.7×10^{-10}	1.0×10^{-9}	2.5×10^{-10}	2.5×10^{-10}
	Sim / Exp	2.23	2.10	2.12	3.08	1.92	1.67
OP1	Exp	4.3×10^{-10}	1.9×10^{-10}	1.7×10^{-10}	3.4×10^{-10}	1.3×10^{-10}	1.5×10^{-10}
	Sim	1.1×10^{-9}	3.6×10^{-10}	3.6×10^{-10}	1.3×10^{-9}	2.5×10^{-10}	2.5×10^{-10}
	Sim / Exp	2.64	1.97	2.11	3.83	1.93	1.66
OP2	Exp	4.2×10^{-10}	1.9×10^{-10}	1.9×10^{-10}	3.4×10^{-10}	1.5×10^{-10}	1.7×10^{-10}
	Sim	8.9×10^{-10}	3.9×10^{-10}	3.9×10^{-10}	1.1×10^{-9}	2.5×10^{-10}	2.5×10^{-10}
	Sim / Exp	2.11	2.08	2.03	3.06	1.69	1.44

simulations and experiments were observed for segment L3L2 irrespective of the presence of the PTO system but not for segment L1S1.

A redistribution of the force range histogram was observed in L1S1. Smaller-range force cycles were observed more frequently in the simulation results than in the experiments owing to the implementation of the mooring segments in the numerical model. A visual observation (through post-processed animations) revealed an oscillating jack-knife behaviour at the joint between the wire and spring. In the numerical model, although the wire and springs were modelled separately, they were nevertheless modelled as solid beam elements. In reality, water passing through the spring will create a damping effect and smooth out the deformation of the entire segment. Whilst the force cycles overpredicted by the numerical simulation will lead to an overprediction of the fatigue damage, the impact is deemed minor because the corresponding force ranges of these force cycles are small.

Mid-range force cycles were observed more frequently in the experiment than in the simulation. This finding was related to the observed vortex-induced motions (VIMs), which could not be predicted by the numerical simulation. The limitation of the numerical simulation could infer an underprediction of the fatigue damage by the current numerical methods if the structures exhibit strong VIM responses. Future work is needed to develop an appropriate method to assess and quantify the importance of VIM and its impact on the fatigue damage of mooring lines.

Considering all the discrepancies, one can observe a better, albeit minor, prediction by the simulation for the overall distribution of the force cycles and, especially, the cycles with a high force range—the cycles that have a large impact on the fatigue damage prediction—in case $OP1_n$. To more precisely quantify the predictive capability of the simulation, fatigue damage accumulation estimations based on these identified load cycles were performed and are presented in Table 4; the results in Table 4 are consistent with the observations in Figure 12.

Table 4 shows that the numerical simulation overpredicted the fatigue damage in the moorings for all segments because the simulation overestimated the motion response of the WEC buoy. As discussed in Yang et al. (2018), the average ratios of the estimated significant motion of the WEC buoy between the simulation and experiment for all OP1-related cases are 1.64 and 1.85 in the surge and heave directions, respectively. In contrast, the respective ratios were found to be 1.08 and 1.35 for OP2. Provided with the knowledge regarding the discrepancy found in the simulated buoy motion, the trends and magnitudes of the results for the irregular loading cases were determined to be reasonable.

With all the estimated fatigue damage from numerical simulations within a factor of 4 the experimental value, which is substantially lower than 10 as recommended in Aker Offshore Partner (1999) and DNV (1992), the proposed numerical methodology demonstrates its capability to be used with confidence for the mooring force response analyses in the following fatigue

assessment, even without performing the calibration. From the standpoint of the practical usage of the numerical models, the current observed prediction discrepancy may also be deemed less pernicious than other issues because the prediction is on the conservative side of the structural safety evaluation. Limitations of the methodology and deficiency of the experiments were, however, also identified; these can be used as guidance for model development in the future or for other researchers if a similar validation experiment is to be performed.

4. Predictive capability of the numerical model for the full-scale installation

As mentioned in Section 1, a prototype device, WaveEL, was installed by the company Waves4Power at full scale for proof of concept in early 2016 (Waves4Power 2019). Measurements were recorded from the operational system from June to November 2017. Readers are referred to Ringsberg et al. (2019) and Yang (2018) for the comprehensive details of the full-scale installation. Because the measurements were taken with various reference coordinates and sampling frequencies and the environmental conditions were not recorded during the measurement period, methodologies were developed to process the measurement data and to identify the environmental loads imparted on the WEC system. A complete description of the methodology and investigation of the measurement results are presented in Ringsberg et al. (2019). In this paper, an adaption of the validated simulation procedure and model to the full-scale WEC installation was performed to assess the model's predictive capability against the full-scale measurement results of the mooring force responses. The model adaption will be presented in Section 4.1, followed by a comparison of the results in Section 4.2.

4.1. Simulation model for the full-scale installation

The numerical model of the full-scale installation was built following the modelling principles presented in Yang (2018). The model was defined according to the installed (full) scale and consisted of a WEC buoy, a three-leg taut mooring system, a power cable and a hub located at a spatially fixed point. Although minor motions of the hub could be observed from the measurement data, it was assumed that the hub could be considered and modelled as a stationary object. The complete set of the properties of the installed WEC system considered in the numerical model can be retrieved from Yang (2018). No calibration of the numerical model was performed. Hence, a heritage of all the limitations identified in the numerical model through the validation study (see Section 3) was expected. The purpose was to examine the changes in the model's predictive capability when transitioning from a well-controlled laboratory environment to a realistic ocean environment, which encompassed a high degree of uncertainty.

The stationary sea states of respective measurement instances, which are represented solely by H_s, T_p, and θ_w, were the research outcomes from Ringsberg et al. (2019). Due to the presence of near-shore currents and tides at the installation site, three-hour stationary seas rarely occurred, and it was concluded that one hour is a more suitable duration for comparison of the results. In total, 35 one-hour stationary periods were identified. The sea states of these 35 independent periods cover H_s values ranging from 0.8-5.5 m, T_p values ranging from 7.7-15.2 s, and θ_w values ranging from 280-340° (where 0° and 240° are the directions heading into Moor1 and Moor2, respectively, and the angles are measured contrac-lockwise). This information was fed into the current study and served as the basic input to the environmental load modelling in the numerical simulations. Each sea state was simulated using the JONSWAP spectrum, wherein γ was set to 2.4 following the recommendations by DNV GL (2017). Finally, the corresponding measurement data and results from the numerical simulation were compared in this study.

The mooring line forces were measured by Dacell CLM-T50 compression load cells with a measurement accuracy of 10 N. The load cells measured the compression between the moving sledge with a mooring bollard structure and the fixed structure welded to the buoy's hull; see the illustration of the installation in Figure 13. The mooring line forces were measured at the fairlead points of the WEC; hence, the mooring line forces obtained from the numerical model were presented in the same locations. Force measurements were available only for the two moorings, Moor1 and Moor2, because a malfunction was found in the load cell on the third mooring. The mooring forces were measured using Dacell compression load cells at a sampling frequency of 60 Hz. Ideally, the force ranges of the load cycles from the time history should be compared, as was done in Section 3. However, only the mean values of the mooring line forces for every one-hour result were compared and presented herein because the measurement accuracy of the load cell was found to be rather low. It was determined that the other response properties were not reliable in the comparison.

4.2. Results for the full-scale installation

Figure 14 presents a comparison of the simulated and measured mooring forces under various sea state conditions. For all 35 simulated cases, on average, the simulated forces were 10% and 15% higher than the measured forces in Moor1 and Moor2, respectively. The difference in the level of agreement was attributed to the uncertainty in θ_w. The sea states used in this study were identified from hindcast data (CMEMS 2017), which predicted θ_w values ranging from 280-340°, whereas a short period of motion measurement of the WEC buoy indicates that the most plausible θ_w values range from 0-60° due

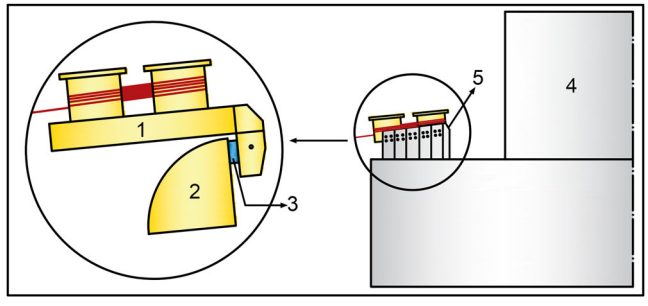

Figure 13. Illustration of the pressure sensor installation: (1) bollard structure, (2) fixed structure, (3) pressure sensor, (4) WEC buoy, and (5) moving sledge.

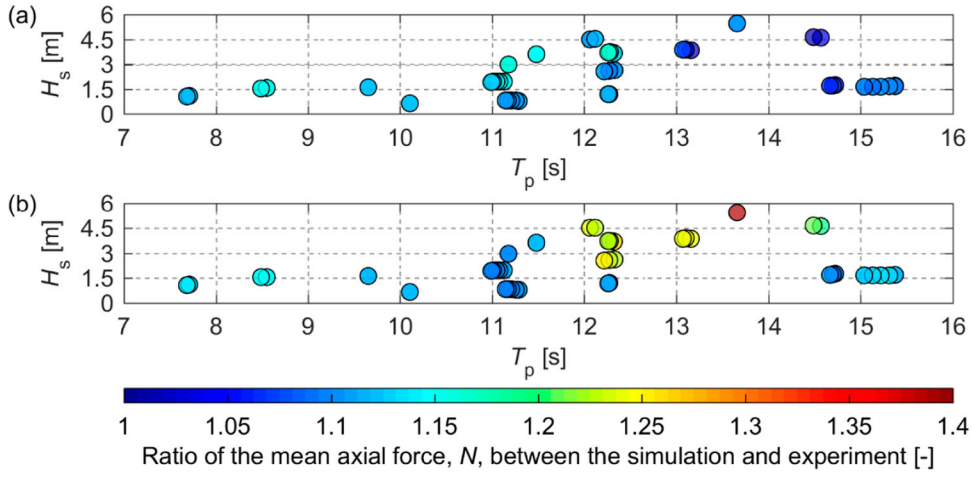

Figure 14. Comparison of the estimated mean force of (a) Moor1 and (b) Moor2 for different sea states. All values are shown as the ratio between the value determined by numerical simulation and measured for the full-scale installation.

to the presence of near-shore currents and tides at the installation site. The investigation in Yang (2018) has shown that θ_w can have a large impact on the prediction of mooring forces. The details of the uncertainty analysis are presented in Ringsberg et al. (2019). In the cited reference, suggestions for the improvement in, e.g. full-scale measurement and sea state monitoring and identification, were also thoroughly discussed.

The discrepancy between the numerical simulation and measurement increases with increases in H_s and T_p; therefore, the region where the WEC system exhibits distinct nonlinear responses must be determined, and a calibration of the system's damage must be performed (Section 3.2). Without the calibration performed in the study and provided with all uncertainties, the presented results demonstrate that the numerical simulation model's predictive ability can be considered good.

5. Conclusions

This study presents a validation of a numerical simulation model against a physical model tested in a laboratory ocean basin experiment. The physical model was made on a 1:20 scale and consists of a WEC buoy, a three-leg two-segment mooring system with submerged floats, and a PTO system designed as a heave plate. The validation primarily regarded the force responses of the moorings, following the first part of the validation concerning the simulated buoy motion presented in Yang et al. (2018).

The simulated force range was in accordance with the experiments for the lower segments in the mooring systems, wherein the average relative difference was 20%. However, discrepancies were found in the force responses of the upper mooring segment due to the uncertain properties of the experimental PTO system. In addition, model limitations were identified, such as linearised drag damping and inability to simulate certain phenomena (e.g. overtopping and vortex-induced motion). Nonetheless, calculations of the fatigue damage based on the force responses in the time domain showed that the simulation model was able to predict the moorings' fatigue within the associated uncertainty level of fatigue, and hence, the goal of the validation study was achieved.

The predictive capability of the numerical model was further examined by adapting the numerical model to a full-scale installation. After moving from a well-controlled laboratory environment to field conditions with uncertainties, an average difference of 13% was found between the simulated force responses and measurements. Overall, it was concluded that the numerical model can be used to support structural (fatigue) safety analyses for moorings under moderate load conditions, whereas special care is required when the system exhibits nonlinear responses, particularly under resonant or severe loading conditions.

Acknowledgements

The authors gratefully acknowledge the financial support provided by the Swedish Energy Agency for the project entitled 'Simulation model for operation and maintenance strategy of floating wave energy converters - analysis of fatigue, wear, and influence of biofouling for effective and profitable energy harvesting' through Contract No. P36357-2. We also thank PhD Filip Alm, MSc Lennart Claesson, and the Swedish company Waves4Power (https://www.waves4power.com/) for providing the WEC system configuration to the authors for designing the experiments.

Disclosure statement

No potential conflict of interest was reported by the author(s).

Funding

This work was supported by Swedish Energy Agency: [Grant Number Contract No. P36357-2].

ORCID

Shun-Han Yang http://orcid.org/0000-0002-6697-4946
Jonas W. Ringsberg http://orcid.org/0000-0001-6950-1864
Erland Johnson http://orcid.org/0000-0003-2397-0643
Zhiqiang Hu http://orcid.org/0000-0003-0806-7616

References

Acxess Spring. 2019. Spring calculator & instant quote. Acxess Spring; [accessed 2019 Feb 8]. https://www.thespringstore.com/spring-calculator-types.html.

Aker Offshore Partner AS. 1999. Target levels for reliability-based assessment of offshore structures during design and operation. Sandsli: Aker Offshore Partner A.S.
Antonutti R, Peyrard C, Incecik A, Ingram D, Johanning L. 2018. Dynamic mooring simulation with Code_Aster with application to a floating wind turbine. Ocean Eng. 151:366–377.
Azcona J, Munduate X, González L, Nygaard TA. 2017. Experimental validation of a dynamic mooring lines code with tension and motion measurements of a submerged chain. Ocean Eng. 129:415–427.
Bosma B, Thiebaut F, Sheng W. 2015. Comparison of a catenary and compliant taut mooring system for marine energy systems. Proceedings of the 11th European Wave and Tidal Energy Conference (EWTEC 2015), 6-11 September, Nantes, France.
Buckham BJ, Nahon M. 2001. Formulation and validation of a lumped mass model for low-tension ROV tethers. Int J Offshore Polar Eng. 11(04):8.
Burgess JJ. 1992. Bending stiffness in a simulation of undersea cable deployment. Proceedings of the Second International Offshore and Polar Engineering Conference (ISOPE1992); 14-19 June; San Francisco, CA, USA.
Casaubieilh P, Thiebaut F, Sheng W, Bosma B, Retzler C, Shaw M, Letertre Y. 2014. Performance improvements of mooring systems for wave energy converters. Progress in Renewable Energies Offshore—Proceedings of the 1st International Conference on Renewable Energies Offshore (RENEW2014), 24-26 November, Lisbon, Portugal. London: Taylor & Francis Group.
Chakrabarti SK. 1987. Hydrodynamics of offshore structures. Dorchester: Springer-Verlag. Chapter 6, Wave force on small structures; p. 168-231.
CMEMS. 2017 Jun - Nov. Data from: Atlantic - European north west shelf - ocean wave analysis and forecast [dataset]. Copernicus Marine Environment Monitoring Service (CMEMS). [accessed 2017 Nov 30]. http://marine.copernicus.eu/services-portfolio/access-to-products/?option=com_csw&view=details&product_id=NORTHWESTSHELF_ANALYSIS_FORECAST_WAV_004_012.
DNV. 1992. Classification notes no. 30.6 structural reliability analysis of marine structures. Det Norske Veritas Classification AS (DNV).
DNV GL. 2015. Offshore standard DNVGL-OS-E301 position mooring. Høvik: DNV GL AS.
DNV GL. 2017. Recommended practice DNVGL-RP-C205 environmental conditions and environmental loads. Høvik: DNV GL AS.
DNV GL. 2019. SESAM software products overview. DNV GL AS; [accessed 2019 Feb 8]. https://www.dnvgl.com/software/products/sesam-products.html.
Dowling NE. 2013. Mechanical behavior of materials: Engineering methods for deformation, fracture, and fatigue. Westford, MA: Angshuman Chakraborty. Chapter 9, Fatigue of materials: Introduction and stress-based approach; p. 416-490.
Fitzgerald J, Bergdahl L. 2007. Considering mooring cables for offshore wave energy converters. Proceedings of 7th European Wave Tidal Energy Conference (EWTEC2007), 11-13 September, Porto, Portugal.
Hall M, Buckham B, Crawford C. 2014. Evaluating the importance of mooring line model fidelity in floating offshore wind turbine simulations. Wind Energy. 17(12):1835–1853.
Hall M, Goupee A. 2015. Validation of a lumped-mass mooring line model with DeepCwind semisubmersible model test data. Ocean Eng. 104:590–603.
Harnois V, Weller SD, Johanning L, Thies PR, Le Boulluec M, Le Roux D, Soulé V, Ohana J. 2015. Numerical model validation for mooring systems: Method and application for wave energy converters. Renewable Energy. 75:869–887.
Holmes B. 2009. Tank testing of wave energy conversion systems: Marine renewable energy guides. London: European Marine Energy Centre.
ITTC. 2014. ITTC – recommended guidelines: Wave energy converter model test experiments. International Towing Tank Conference (ITTC).
KYOWA. 2019. Lux-b-id compact tension/compression load cell. KYOWA; [accessed 2019 July 8]. https://www.kyowa-ei.com/eng/product/category/sensors/lux-b-id/index.html.
Martin T, Schacht S, Riesen P, Paschen M. 2018. Efficient implementation of a numerical model for flexible net structures. Ocean Eng. 150:272–279.
Ormberg H, Stansberg CT, Yttervik R, Kleiven G. 1999. Integrated vessel motion and mooring analysis applied in hybrid model testing. Proceedings of the 9th International Offshore and Polar Engineering Conference (ISOPE1999); 30 May - 4 June; Brest, France. International Society of Offshore and Polar Engineers.
Paredes GM, Palm J, Eskilsson C, Bergdahl L, Taveira-Pinto F. 2016. Experimental investigation of mooring configurations for wave energy converters. Int J Marine Energy. 15:56–67.
Paschen M, Niedzwiedz G, Winkel H-J. 2004. Fluid structure interactions at towed fishing gears. ASME 2004 23rd International Conference on Offshore Mechanics and Arctic Engineering (OMAE2004), 20–25 June, Vancouver, British Columbia, Canada. New York.
Payne GS, Taylor JRM, Ingram D. 2009. Best practice guidelines for tank testing of wave energy converters. J Ocean Technol. 4(4):38–70.
Pecher A, Kofoed JP. 2017. Handbook of ocean wave energy. Switzerland: Springer International Publishing. https://doi.org/10.1007/978-3-319-39889-1.
Ringsberg JW, Yang S-H, Lang X, Johnson E, Kamf J, Guedes Soares C. 2019. Mooring forces in a floating point-absorbing WEC system - a comparison between full-scale measurements and numerical simulations. Proceedings of the International Conference on Ships and Offshore Structures (ICSOS2019), 4-8 November, Florida, USA.
Rychlik I. 1987. A new definition of the rainflow cycle counting method. Int J Fatigue. 9(2):119–121.
SINTEF Ocean. 2018. RIFLEX 4.14.0 theory manual. SINTEF Ocean: Trondheim.
SJTU. 2019. State key laboratory of ocean engineering. Shanghai: Shanghai Jiao Tong University (SJTU). [accessed 2019 Feb 19]. http://en.sjtu.edu.cn/research/centers-labs/state-key-laboratory-of-ocean-engineering.
Stansberg C, Øritsland O, Kleiven G. 2000a. VERIDEEP: Reliable methods for verification of mooring and stationkeeping in deep water. Proceedings of the Offshore Technology Conference (OTC2000); 1-4 May; Houston, TX, USA.
Stansberg C, Yttervik R, Oritsland O, Kleiven G. 2000b. Hydrodynamic model test verification of a floating platform system in 3000 m water depth. Proceedings of the ETCE/OMAE2000 Joint Conference Energy for the New Millennium; 14 -17 February; New Orleans, Louisiana. American Society of Mechanical Engineers.
Waves4Power. 2019. Installation of the WaveEL buoy on site at Runde. Gothenburg: Waves4Power; [accessed 2019 Feb 8]. http://www.waves4power.com/uncategorized/installation-of-the-waveel-buoy-on-site-at-runde/.
Xu S, Ji C, Guedes Soares C. 2018. Experimental study on taut and hybrid moorings damping and their relation with system dynamics. Ocean Eng. 154:322–340.
Yang S-H. 2018. Analysis of fatigue characteristics of mooring lines and power cables for floating wave energy converters [dissertation]. Gothenburg: Chalmers University of Technology.
Yang S-H, Ringsberg JW, Johnson E, Hu Z, Bergdahl L, Duan F. 2018. Experimental and numerical investigation of a taut-moored wave energy converter: A validation of simulated buoy motions. Proceedings of the Institution of Mechanical Engineers, Part M: Journal of Engineering for the Maritime Environment. 232(1):97–115.
Yang S-H, Ringsberg JW, Johnson E, Hu Z, Palm J. 2016. A comparison of coupled and de-coupled simulation procedures for the fatigue analysis of wave energy converter mooring lines. Ocean Eng. 117:332–345.

Appendix A. Main properties of the studied WEC system for the laboratory test

Table A1. Basic properties of the WEC buoy.

	Full-scale prototype	1:20 model
Mass [kg]	451.751	55.092
Draft [m]	34.9	1.745
CoG [m]*	(0, 0, −14.1)	(0, 0, −0.705)
Roll, pitch, and yaw inertia relative to the CoG [kgm^2]	5.160×10^7, 5.160×10^7, 2.154×10^5	15.732, 15.732, 6.566×10^{-2}

* The origin of the reference Cartesian coordinate is placed on the plane of the water surface at the geometric centre of the WEC buoy when the buoy is in its unloaded neutral position.

Table A2. Properties of the PTO system; values are presented in the model scale (1:20) except as otherwise noted.

Dimensions of the heave plate, length×width×height [m×m×m]	0.21×0.21×0.005
Dimensions of the connection bar, length×diameter [m×m]	0.658×0.19
Unloaded length of one spring [m]	0.617
End stiffness of the two spring [N/m]	5.88
Pretension force of the spring [N]	3.242
Target linear damping of the PTO system in the prototype scale [Ns/m]	3.315×10^4
Target linear damping of the PTO system in the model scale [Ns/m]	18.081
Equivalent linear damping of the heave plate [Ns/m]	18.079

Table A3. Properties of the mooring system.

	Full-scale prototype	1:20 model
Depth of the anchor [m]	80	4.0
Radius of the anchor [m]	125.109	6.255
Height of the fairlead [m]*	1.125	0.056
Pretension force at the fairlead [N]	2.200×10^4	2.683
Dry mass of each segment [kg/m]	4.9	–**
Submerged weight of each segment [N/m]	35.868	0.087
Nominal diameter of each segment [m]	0.08	–**
Axial stiffness of each segment [N]	5.754×10^6	701.671***
Lengths of segments S1 and S2 [m]	92.7, 69.745	4.635, 3.487
Mass of the spring [kg/m]	–****	0.211
Nominal (outermost) diameter of the spring [m]	–****	0.011
Thread diameter of the spring [mm]	–****	1.5
Lengths of springs Sp1 and Sp2 [m]	–****	0.210, 0.143
End stiffnesses of springs Sp1 and Sp2 [N/m]	–****	126, 185
Mass of the steel wire [g/m]	–****	13.8
Diameter of the steel wire [mm]	–****	0.83
Axial stiffness of the steel wire [kN]	–****	50.0
Lengths of steel wires Wi1 and Wi2 [m] *****	–****	4.790, 3.344
Mass of the float [kg] ******	2900	0.354
Height of the float [m]	3.6	0.180

* Measured from the upper deck.
** Defined for the spring and steel wire, respectively.
*** The target design value for the combined equivalent stiffness when one spring and one steel wire are connected.
**** Not used in the full-scale prototype.
***** The length is referred to as the stretched length, whereas the final installed length of Wi1 is adjusted when the target pretension force at the fairlead is achieved.
****** The CoG of the float is located at the geometrical centre of the float, and the moment of inertia of the float was not modelled in the experiment.